The effect of a movable mass on the aeroelastic stability of composite hingeless rotor blades in hover

M.R. Amoozgar*, A.D. Shaw†, J. Zhang*, M.I. Friswell‡

College of Engineering, Swansea University, Swansea, Wales SA2 8PP, United Kingdom

Abstract

In this paper, the aeroelastic stability of a composite hingeless rotor blade with a chordwise movable mass is investigated. The point mass is located near the tip of the blade and its chordwise location is variable with respect to the elastic axis and can be moved during the flight. This movable mass is added to the blade to actuate the blade twist during flight. By actuating the mass in the chord direction of the blade during the flight, a bending moment which is the result of the centrifugal force of the mass and its offset is induced on the blade. This bending moment induces twist in the blade, due to bend-twist coupling in the composite lamination. The blade is modelled by using the geometrically exact fully intrinsic beam equations along with the variational asymptotic beam sectional analysis. The aerodynamic loads are simulated by using the two-dimensional strip theory combined with a uniform inflow. The nonlinear partial differential aeroelastic equations are discretized by a time-space scheme, and the converged results are compared with those reported in the literature and a very good match is observed. The results show that by positioning the mass near the tip of the blade, and also by using the ply angle of about 30 degree in this configuration, the highest possible twist change is achieved when the mass moves from the leading edge to the trailing edge of the blade. Moreover, the spanwise location of the mass slightly changes the stability boundaries, while the chordwise movement significantly affects the aeroelastic instability.

Keywords: Morphing blade, Aeroelastic stability, composite material, bend-twist coupling, fully intrinsic equations, concentrated mass.

*Postdoctoral Research Assistant, College of Engineering, Swansea University, UK
†Lecturer, College of Engineering, Swansea University, UK
‡Professor, College of Engineering, Swansea University, UK

Introduction

During the past decades of development in rotorcraft industry, different concepts have been suggested to enhance the performance of the vehicle and at the same time to decrease the pollution, noise and vibration, by changing the shape of the blade. Blade twist morphing is a concept which could modify the shape of the blade in flight to achieve the best performance in each flight condition. For helicopter rotors, the twist distribution that minimizes the power requirement is different in each flight condition [1]. Therefore, the predefined blade twist variation normally is chosen as a compromise between different flight conditions. Blade twist morphing changes the blade twist during flight to allow the rotorcraft to fly in an optimum condition in terms of twist variation. Han et al. [2] showed how the performance of a helicopter during flight could be improved by dynamic blade twist. They demonstrated that the dynamic blade twist improves the performance and reduces the rotor power requirement. Chen and Chopra [3] studied the effect of piezoelectric actuators on the twist change of blades. The piezoelectric patched were positioned on the top and bottom of the blade and about 0.4^{o} of twist change was achieved. Then this concept was tested in hover condition, and it was proved that a linear twist change of about 0.6^{o} can modify the rotor lift by 10% [4]. Reduction and control of the vibratory loads of a composite box beam blade with using the smart materials was considered by Chattopadhyay et al. [5]. It was found that the number of actuators and their location have significant effect on the reduction of dynamic loads. Cesnik et al. [6] developed an analytical model for modelling an active twist rotor blade with distributed anisotropic strain actuators. This active twist rotor aimed to reduce the vibration and noise of the blade, and good correlation with experiments was observed. This study developed further to cover the forward flight condition by Shin and Cesnik [7]. Prashant and Sung [8] analysed how the active twist concept affect the active vibration reduction of composite blades with imperfections. They showed that the rotor vibratory loads and also the energy input may be influenced by introducing imperfections to the blade. Twist distribution modification of a tiltrotor blade based on shape memory alloy torque tube was studied by Prahlad and Chopra [9]. In this study, the actuation behaviour was tuned by the heat treatment of SMAs. Mistry et al. [1] developed a warp-induced twist variation concept for rotary-wing applications. In this method, the

twist of the blade changes by rotation of a threaded rod. More recently, Amoozgar et al. [10, 11] developed a novel concept for twist morphing of composite blades. In this study, the twist of the blade was the result of mass movement and stiffness tailoring of the composite blade.

Aeroelastic analysis of helicopter rotor blades is a key design requirement. Hingeless rotor blades are normally considered as cantilevered beams, and the common type of aeroelastic instability is the one characterized by the coupling between lead-lag bending, flap bending, and torsion deflections of blades. The frequency of this instability is usually near to the lead-lag natural frequency [12]. There are some review papers dedicated to surveying different models used for composite rotor blade analysis [13]. One of the first studies concerning with the aeroelastic stability of composite rotor blades, was considered by Hong and Chopra [14]. It was found that depending on the laminate design of the box beam, different stability characteristics may be obtained. Panda and Chopra [15] determined the aeroelastic stability and response of composite hingeless rotor blades based on moderate deflection beam theory in forward flight. The effect of ply orientation and elastic coupling on the vibration and stability was shown. The effect of transverse shear deformation on the modelling of the rotor blade for aeroelastic analysis and response of composite rotors has been presented by Smith and Chopra [16] in forward flight. They also showed that the unsteady aerodynamic increases the vibratory load up to 30%. Kim and Dugundji [17] investigated the large amplitude, nonlinear aeroelastic behaviour of composite hingeless rotor blades in hover condition. Numerical results showed that in moderate amplitude, the nonlinear aerodynamics is dominant, and nonlinear static-dynamic structural couplings can affect the aeroelastic behaviour at large amplitudes. The aeroelastic response and vibratory loads of an elastically tailored composite rotor blade has been determined by Smith [18]. It was highlighted that the positive or negative elastic couplings have stabilizing or destabilizing effect on the lag mode damping. Tracy and Chopra [19] studied the aeroelastic stability of a composite hingeless rotor blade in hover flight. In the positive collective pitch angles, the lag damping mode stabilizes with negative chordwise bending-torsion coupling. The influence of fibre orientation and stacking sequence on the aeroelastic stability of composite rotor blades has been

investigated by Jeon et al. [20]. The lag mode instability is influenced by the bending-twist coupling in the symmetric lamination, and the extension-twist coupling in the antisymmetric configuration.

A new formulation based on exact beam formulation and unsteady dynamic wake aerodynamic model was considered by Shang et al. [21] for aeroelastic stability analysis of composite hingeless rotor blades. The initial twist and curvature of the composite blade can improve the aeroelastic stability and reduce the static loads. Jeon and Lee [22] considered the aeroelasticity of a composite rotor blade using a finite element method based on large deflection beam theory in forward flight. It was proposed that when the deflection is large, the full finite element should be used instead of modal approach to predict the stability behaviour accurately. An analytical model for investigating the aeroelasticity of composite blades with swept tips was proposed by Friedmann et al. [23]. The tip sweep can have destabilizing effect on the blade, while this instability can be removed in some certain ply angles of the composite blade. Bao et al. [24] designed and tested several Mach scaled composite blades to reduce the vibratory loads of the blade and good correlation in hover condition was observed. Friedmann et al. [25] examined the compatibility between the composite cross-sectional analysis based on variational asymptotic approach and a moderate deflection beam model, and the results were validated with experimental data. The aeroelastic stability behaviour of an isolated composite hingeless rotor blade has been determined by Fulton and Hodges [26]. The blade was modelled by a geometrically exact beam formulation without any restrictions on the rotations and displacements magnitudes. The analysis showed that the non-classical couplings affect the aeroelastic stabilities, and therefore must be considered in general purpose analysis. Lim and Lee [27] studied the aeroelastic analysis of bearingless rotor blades considering a composite flexbeam by using a large deflection beam theory. They showed that the bending-torsional coupling of the composite layup could change the stability of the lag mode. The aeroelastic stability of composite hingeless rotors by using the free-wake aerodynamic model has been also considered by Xiao et al. [28].

Byers and Gandhi [29-31] explored the influence of a moving mass in the spanwise direction on the aeroelastic stability to produce a vibration absorber. They showed the Coriolis forces couple the flapping and the lead-lag motion together and hence affect the rotor stability. The effect of embedded

chordwise absorbers on the stability of the rotor system was studied experimentally and analytically by Kang et al. [32]. They showed that using the chordwise absorbers improves the stability of rotors.

To add to the aforementioned literature, in this study a new twist morphing concept based on the mass movement is introduced, and the effect of this morphing concept on the aeroelastic stability boundaries of the composite hingeless rotor blade in hovering condition is determined. The blade structural model is based on the geometrically exact fully intrinsic beam equations [33] and the aerodynamic loading on the blade is a combination of the quasi-steady strip aerodynamic theory and the uniform inflow [34]. The added mass is modelled as a concentrated mass attached to the blade which can move in different directions [10], and the cross-sectional characteristics are determined by using the variational asymptotic approach [35].

Problem Statement

A composite hingeless rotor blade is modelled here as a cantilevered beam attached to the blade hub. The blade has a composite rectangular closed box section as a spar. The blade is equipped with a track attached to the spar to allow for point mass chordwise movement in flight. This mass movement produces a variable in-plane bending moment due to the centrifugal force acting on the mass. This bending moment then turns to an equivalent torsional moment through the spar lag-torsion coupling. Therefore, the twist of the blade depends on the point mass chordwise movement. The point mass location along the blade coordinate system is denoted here as x_p and y_p, respectively. Figure 1 shows a schematic of the morphing system described above. The chordwise position of the mass (y_p), shown in Figure 1, is able to change in flight and assumes a suitable mechanism may be designed. Thus, when the flight condition changes, the required blade twist, in terms of the optimum performance, changes. The spanwise location of the added mass is a fixed design variable. It is assumed that the added mass doesn't have any offset in the z direction (z_p=0). The origin of the coordinate system is located at the root of the blade and on the quarter chord of the section. The x axis is along the blade span, and the y axis is along the chord of the blade toward the leading edge of the blade.

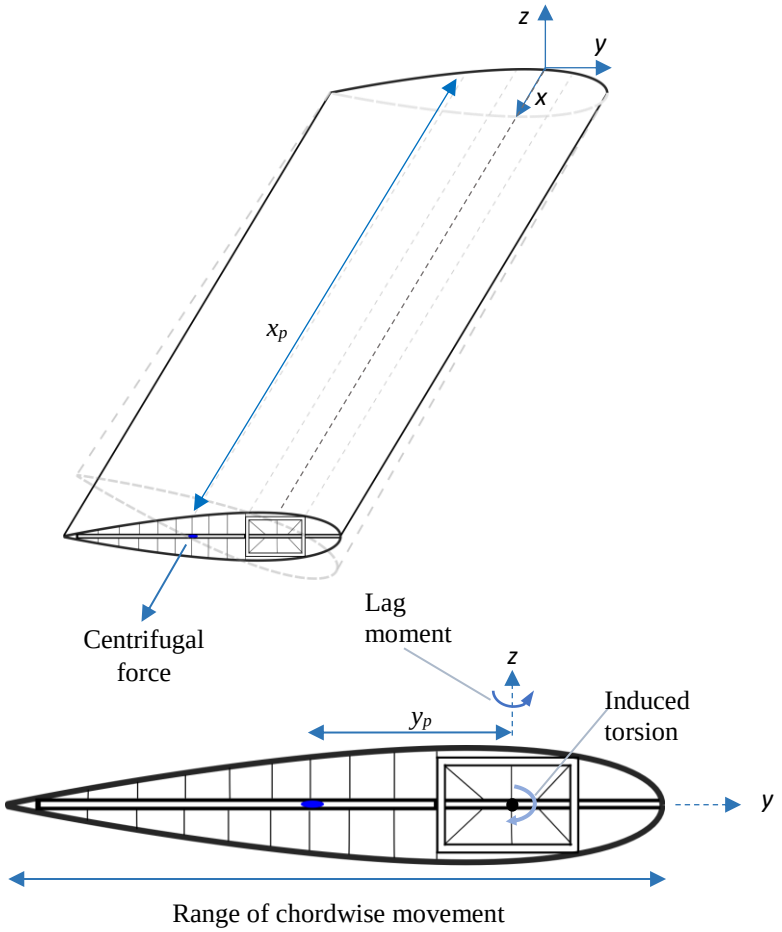

Figure 1: Schematic of the morphing twist change concept

Aeroelastic Modelling

The aeroelastic modelling of the blade is composed of two modules, the structural model and the aerodynamic loading model. The three-dimensional structural model of the blade can be divided into two parts. In the first part, a two-dimensional cross-sectional analysis is carried out by using the variational asymptotic approach [35], and the cross-sectional properties are obtained. Then the global behaviour of the blade is modelled by the one-dimensional nonlinear geometrically exact fully intrinsic beam equations [33]. This formulation has been successfully used for structural analysis of stationary and rotating beams [36-38].

The geometrically exact fully intrinsic beam equations express the nonlinear behaviour of generally anisotropic, initially twisted and curved beam as

$$\partial F_1/\partial x_1 + K_2F_3 - K_3F_2 + f_{aero_1} = \partial P_1/\partial t + \Omega_2P_3 - \Omega_3P_2$$

$$\partial F_2/\partial x_1 + K_3F_1 - K_1F_3 + f_{aero_2} = \partial P_2/\partial t + \Omega_3P_1 - \Omega_1P_3$$

$$\partial F_3/\partial x_1 + K_1F_2 - K_3F_1 + f_{aero_3} = \partial P_3/\partial t + \Omega_1P_2 - \Omega_2P_1$$

$$\partial M_1/\partial x_1 + K_2M_3 - K_3M_2 + 2\gamma_{12}F_3 - 2\gamma_{13}F_2 + m_{aero_1} = \partial H_1/\partial t + \Omega_2H_3 - \Omega_3H_2 + V_2P_3 - V_3P_2$$

$$\partial M_2/\partial x_1 + K_3M_1 - K_1M_3 + 2\gamma_{13}F_1 - (1+\gamma_{11})F_3 + m_{aero_2} = \partial H_2/\partial t + \Omega_3H_1 - \Omega_1H_3 + V_3P_1 - V_1P_3$$

$$\partial M_3/\partial x_1 + K_1M_2 - K_2M_1 + (1+\gamma_{11})F_2 - 2\gamma_{12}F_1 + m_{aero_3} = \partial H_3/\partial t + \Omega_1H_2 - \Omega_2H_1 + V_1P_2 - V_2P_1$$

$$\partial V_1/\partial x_1 + K_2V_3 - K_3V_2 + 2\gamma_{12}\Omega_3 - 2\gamma_{13}\Omega_2 = \partial\gamma_{11}/\partial t \quad (1)$$

$$\partial V_2/\partial x_1 + K_3V_1 - K_1V_3 - (1+\gamma_{11})\Omega_3 + 2\gamma_{13}\Omega_1 = 2\partial\gamma_{12}/\partial t$$

$$\partial V_3/\partial x_1 + K_1V_2 - K_2V_1 + (1+\gamma_{11})\Omega_2 - 2\gamma_{12}\Omega_1 = 2\partial\gamma_{13}/\partial t$$

$$\partial\Omega_1/\partial x_1 + K_2\Omega_3 - K_3\Omega_2 = \partial\kappa_1/\partial t$$

$$\partial\Omega_2/\partial x_1 + K_3\Omega_1 - K_1\Omega_3 = \partial\kappa_2/\partial t$$

$$\partial\Omega_3/\partial x_1 + K_1\Omega_2 - K_2\Omega_1 = \partial\kappa_3/\partial t$$

where, x_1 is the spanwise coordinate of the beam reference line, F_i and M_i for i=1,2,3, are the internal forces and moments, V_i and Ω_i are the linear and angular velocities, P_i and H_i are the sectional linear and angular momenta, respectively. K_i is the final curvature of the deformed beam, and γ_{1i} and κ_{1i} are the strain measures. The aerodynamic force and moments on the blade are defined here by f_{aero_i} and m_{aero_i} for i=1,2,3. All these parameters are defined in the deformed coordinate system except the initial curvature. The details of the formulation can be found in [33]. The cross-sectional properties of the composite spar is determined by VABS [35], which are then introduced in the beam formulation through the stiffness matrix as

$$\begin{bmatrix} F_1 \\ F_2 \\ F_3 \\ M_1 \\ M_2 \\ M_3 \end{bmatrix} = \begin{bmatrix} A_{11} & A_{12} & A_{13} & B_{11} & B_{12} & B_{13} \\ A_{12} & A_{22} & A_{23} & B_{21} & B_{22} & B_{23} \\ A_{13} & A_{23} & A_{33} & B_{31} & B_{32} & B_{33} \\ B_{11} & B_{12} & B_{13} & D_{11} & D_{12} & D_{13} \\ B_{21} & B_{22} & B_{23} & D_{12} & D_{22} & D_{23} \\ B_{31} & B_{32} & B_{33} & D_{13} & D_{23} & D_{33} \end{bmatrix} \begin{bmatrix} \gamma_{11} \\ 2\gamma_{12} \\ 2\gamma_{13} \\ \kappa_1 \\ \kappa_2 \\ \kappa_3 \end{bmatrix} \quad (2)$$

where **A**, **B**, and **D** are the composite spar cross-section stiffness components. It is noted that these stiffness matrices are different from the stiffness matrices obtained based on lamination theory. As the beam is clamped to the root, the fixed boundary conditions are applied to close the formulation.

The aerodynamic loads in the hover condition based on the intrinsic expression of the Greenberg's theory [34] is defined as

$$\boldsymbol{f}_{aero} = \boldsymbol{C}^{Ba}\boldsymbol{f}_a \tag{3}$$
$$\boldsymbol{m}_{aero} = \boldsymbol{C}^{Ba}m_a + \boldsymbol{C}^{Ba}\boldsymbol{x}_a\boldsymbol{f}_a$$

where $\boldsymbol{x}_a$ is the offset between the beam reference line, and the aerodynamic centre, and $\boldsymbol{C}^{Ba}$ is the direction cosine matrix of deformed frame with respect to aerodynamic frame. In this study, it is assumed that the offset of the aerodynamic centre from the elastic axis is zero. The aerodynamic force and moment equations in the aerodynamic reference frame are [34]

$$f_a = \rho_\infty b \begin{bmatrix} 0 \\ c_{l_a}V_{a3}^2 - c_{d_0}V_T V_{a2}^2 + c_{d_a}V_{a_3}V_{a_2} \\ -c_{l_a}V_{a_2}\left(V_{a_3} - \frac{\Omega_a b}{2}\right) - \frac{c_{l_a}\dot{V}_{a_3}b}{2} - c_{d_0}V_T V_{a_3} + c_{d_a}V_{a_3}^2 \end{bmatrix} \tag{4}$$

$$m_a = 2\rho_\infty b^2 \begin{bmatrix} -bc_{l_a}V_{a_2}\Omega_a/8 - c_{l_a}\left(b^2\dot{\Omega}_a/32 - b\dot{V}_{a_3}/8\right) \\ 0 \\ 0 \end{bmatrix}$$

where c_{l_a}, c_{d_0}, and c_{d_a} are the airfoil lift and drag coefficients, respectively. The variables with subscript ($_a$) are expressed in the aerodynamic reference frame. The induced inflow velocity corrects the vertical component of the velocity as follow

$$V_{a_{3T}} = V_{a_3} + \lambda \tag{5}$$

The uniform induced inflow velocity determined by the blade element momentum theory at ¾ span, λ, is given as [39]

$$\lambda = sgn[\theta + \phi(0.75R)]\frac{\pi\sigma}{8}\,\Omega R\left(\sqrt{1 + \frac{12}{\pi\sigma}|\theta + \phi(0.75R)|} - 1\right) \tag{6}$$

where σ is the blade solidity, and θ and ϕ are the blade pitch angle and elastic twist angle, respectively.

Finally, by combining the structural and aerodynamic models together, the full aeroelastic equations can be obtained. To solve the nonlinear aeroelastic equations, a time-space discretization scheme is used [33]. In this method, every unknown variable is defined on the right and left hand sides of each node. By applying this scheme to the governing equations, the discretized equations of motion for the n^{th} element in the vector format will be:

$$\begin{aligned}
&\frac{\hat{\mathbf{F}}_{\mathbf{l}}^{\mathbf{n+1}}-\hat{\mathbf{F}}_{\mathbf{r}}^{\mathbf{n}}}{dl}+(\tilde{\overline{\boldsymbol{\kappa}}}^{n}+\tilde{\mathbf{k}}^{n})\overline{\mathbf{F}}^{n}+\overline{\mathbf{f}}_{aero}^{n}=\dot{\overline{\mathbf{P}}}^{n}+\tilde{\overline{\boldsymbol{\Omega}}}^{n}\overline{\boldsymbol{P}}^{n}\\
&\frac{\hat{\mathbf{M}}_{\mathbf{l}}^{\mathbf{n+1}}-\hat{\mathbf{M}}_{\mathbf{r}}^{\mathbf{n}}}{dl}+\left(\tilde{\overline{\boldsymbol{\kappa}}}^{n}+\tilde{\mathbf{k}}^{n}\right)\overline{\mathbf{M}}^{n}+\left(\tilde{\mathbf{e}}_{\mathbf{1}}+\tilde{\overline{\boldsymbol{\gamma}}}^{n}\right)\overline{\mathbf{F}}^{n}+\overline{\mathbf{m}}_{aero}^{n}=\dot{\overline{\mathbf{H}}}^{n}+\tilde{\overline{\boldsymbol{\Omega}}}^{n}\overline{\boldsymbol{H}}^{n}+\tilde{\overline{\mathbf{V}}}^{n}\overline{\boldsymbol{P}}^{n}\\
&\frac{\hat{\mathbf{V}}_{\mathbf{l}}^{\mathbf{n+1}}-\hat{\mathbf{V}}_{\mathbf{r}}^{\mathbf{n}}}{dl}+\left(\tilde{\overline{\boldsymbol{\kappa}}}^{n}+\tilde{\mathbf{k}}^{n}\right)\overline{\mathbf{V}}^{n}+\left(\tilde{\mathbf{e}}_{\mathbf{1}}+\tilde{\overline{\boldsymbol{\gamma}}}^{n}\right)\overline{\boldsymbol{\Omega}}^{n}=\dot{\overline{\boldsymbol{\gamma}}}^{n}\\
&\frac{\hat{\boldsymbol{\Omega}}_{\mathbf{l}}^{\mathbf{n+1}}-\hat{\boldsymbol{\Omega}}_{\mathbf{r}}^{\mathbf{n}}}{dl}+\left(\tilde{\overline{\boldsymbol{\kappa}}}^{n}+\tilde{\mathbf{k}}^{n}\right)\overline{\boldsymbol{\Omega}}^{n}=\dot{\overline{\boldsymbol{\kappa}}}^{n}
\end{aligned} \tag{7}$$

where, subscripts *r* and *l* refer to the right and left hand sides of each node, ($\widehat{\ }$) represents the nodal value of each variable, and ($\tilde{\ }$), the tilde operator, converts any vector to its corresponding matrix. The element variable, ($\overline{\ }$), defines the average of each variable such as **F,** as follows:

$$\overline{\mathbf{F}}^{n}=\frac{\hat{\mathbf{F}}_{\mathbf{l}}^{\mathbf{n+1}}+\hat{\mathbf{F}}_{\mathbf{r}}^{\mathbf{n}}}{\mathbf{2}} \tag{8}$$

In this way, any discontinuity, such as the point mass, can be taken into account. Hence, the following nodal equations are used to consider the nodal mass effect on the equations of motion:

$$\hat{\mathbf{F}}_{\mathbf{r}}^{\mathbf{n}}-\hat{\mathbf{C}}_{\mathbf{lr}}^{\mathbf{n}\,\mathbf{T}}\hat{\mathbf{F}}_{\mathbf{l}}^{\mathbf{n}}+\hat{\mathbf{f}}_{\mathbf{aero}}^{\mathbf{n}}=\dot{\hat{\mathbf{P}}}_{\mathbf{r}}^{\mathbf{n}}+\tilde{\hat{\boldsymbol{\Omega}}}_{\mathbf{r}}^{\mathbf{n}}\hat{\mathbf{P}}_{\mathbf{r}}^{\mathbf{n}} \tag{9}$$

$$\hat{\mathbf{M}}_{\mathbf{r}}^{\mathbf{n}}-\hat{\mathbf{C}}_{\mathbf{lr}}^{\mathbf{n}\,\mathbf{T}}\hat{\mathbf{M}}_{\mathbf{l}}^{\mathbf{n}}+\hat{\mathbf{m}}_{\mathbf{aero}}^{\mathbf{n}}=\dot{\hat{\mathbf{H}}}_{\mathbf{r}}^{\mathbf{n}}+\tilde{\hat{\boldsymbol{\Omega}}}_{\mathbf{r}}^{\mathbf{n}}\hat{\mathbf{H}}_{\mathbf{r}}^{\mathbf{n}}+\tilde{\hat{\mathbf{V}}}_{\mathbf{r}}^{\mathbf{n}}\hat{\mathbf{P}}_{\mathbf{r}}^{\mathbf{n}} \tag{10}$$

where, $\hat{\mathbf{C}}_{\mathbf{lr}}^{\mathbf{n}}$ is the slope discontinuity, and in this case it is simply the identity matrix. The added mass is introduced to the formulation through the generalized momentum-velocity relation as follows:

$$\begin{Bmatrix}\hat{\mathbf{P}}_{r}\\ \hat{\mathbf{H}}_{r}\end{Bmatrix}=\begin{bmatrix}\hat{m}\Delta & -\hat{m}\tilde{\hat{X}}\\ \hat{m}\tilde{\hat{X}} & \hat{I}\end{bmatrix}\begin{Bmatrix}\hat{\mathbf{V}}_{r}\\ \hat{\boldsymbol{\Omega}}_{r}\end{Bmatrix} \tag{11}$$

where, $\hat{m}$, $\hat{I}$, and $\hat{X}$ are the added mass value, moment of inertia, and location from the beam reference line. In this study, the moment of inertia of the added mass ($\hat{I}$) about its centroid is assumed to be zero. The added mass value and its offset from the reference line is zero everywhere except the location at which the mass is added to the blade:

$$\hat{I} = 0, \quad \hat{m}_M = m_p, \quad \hat{X}_M = [0 \quad y_p \quad z_p]^T \tag{12}$$

where *M* is the node at which the mass is added.

First by removing all the time derivatives terms, the steady-state condition of the system is obtained. Then the nonlinear equations are linearized about the steady-state solution, and the aeroelastic frequency and damping are determined from the eigenvalue analysis. The aeroelastic stability of the hingeless rotor blade here is investigated here by checking the lead-lag mode damping as this mode is more prone to suffer from aeroelastic instability due to low values of drag force in this direction [12].

Numerical Results

To check the validity of the developed aeroelastic code, two cases are considered and compared with those reported in the literature. First the effect of adding a tip point mass with a weight equal to the blade weight, on the nondimensional first and second flap modes of an isotropic cantilevered beam is considered. The obtained results are compared with those reported by Wright et al. [40] in Figure 2, and shown to be a good match. Here *m* is the mass per unit length, *R* is the blade length, Ω_0 is the rotating velocity, and EI_2 is the flap bending stiffness of the blade. It is noted that here the added tip mass value is equal to the blade overall mass.

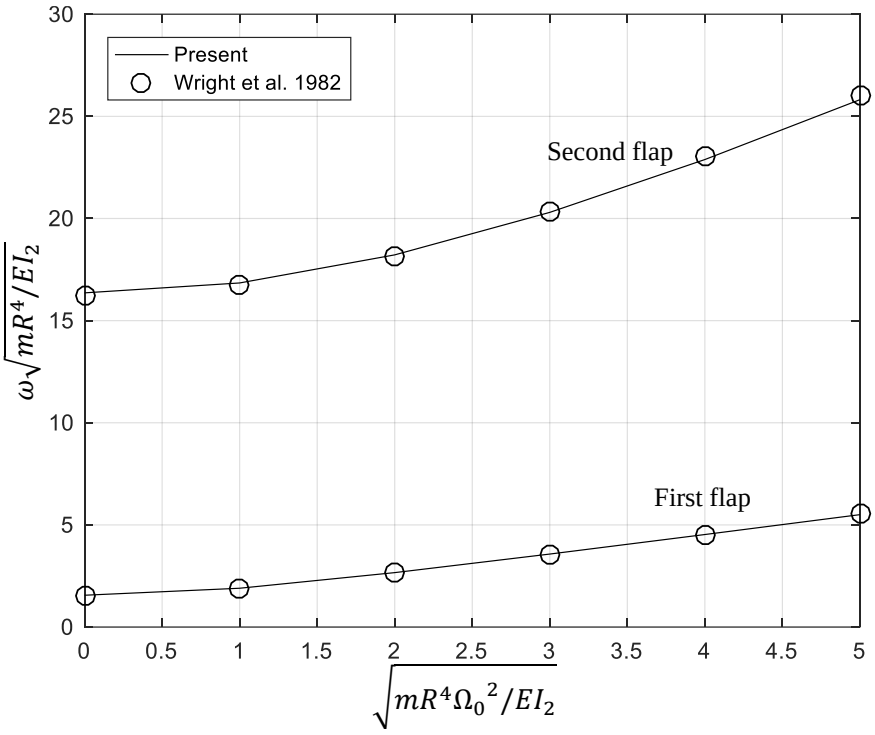

Figure 2: Comparison of the change in frequency parameter with respect to the nondimensional rotating speed for an isotropic beam with a point mass

To check the accuracy of the aeroelastic analysis results, a composite blade identical to the one used in [26] is considered next. The blade spar is a rectangular box section, with outer dimensions of 12.804 mm and 8.944 mm with a wall thickness of 0.804 mm. The spar is made of AS4/3501-6 graphite/epoxy with material properties described in Table 1. Each wall of the spar box has 6 layers of $[0_2, \zeta_4]$ and the layups are antisymmetric with respect to the mid-plane of the cross-section as shown in Figure 3.

Table 1: AS4/3501-6 graphite/epoxy material properties [26]

Material property	**Value**
E_{11} (Gpa)	142
$E_{22} = E_{33}$ (Gpa)	9.81
$G_{12} = G_{13}$ (Gpa)	6
G_{23} (Gpa)	3.77

$v_{12}= v_{13}$	0.3
v_{23}	0.34

The rotor blade characteristics are listed in Table 2. The nondimensional aeroelastic lead-lag damping of this box-beam case is determined for various blade pitch angles, and compared with those obtained by Fulton and Hodges [26] in Figure 3. The Timoshenko sectional stiffness matrices determined by VABS for this case are presented in Table 3.

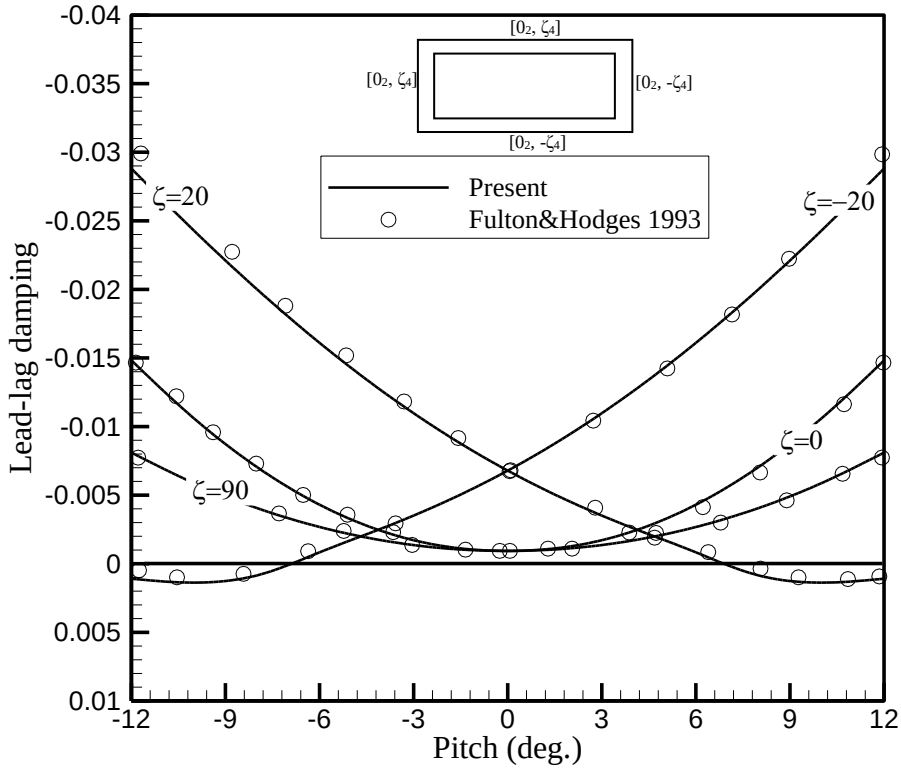

Figure 3: Comparison of the lead-lag damping of the composite blade

Table 2: Hingeless rotor blade characteristics

Parameter	**Definition**	**Value**
$\gamma = 3\rho_\infty c_{l_a} cR/m$	Lock number	5.593
$\sigma = N_b c/\pi R$	Solidity	0.0572
c/R	Chord/blade length	0.08986

N_b	Number of blades	2
c_{d_0}/c_{l_a}	Drag coefficient to lift coefficient ratio	0.0079/6.283

234

235 Table 3: Timoshenko stiffness matrix

Stiffness	ζ=0°	ζ=20°	ζ=90°
A_{11} (N)	4.6×10^6	3.63×10^6	1.68×10^6
A_{22} (N)	1.07×10^5	2.19×10^5	9.95×10^4
A_{33} (N)	6.3×10^4	1.26×10^5	5.54×10^4
B_{11} (N.m)	0	3.37×10^3	0
B_{22} (N.m)	0	1.64×10^3	0
B_{33} (N.m)	0	1.66×10^3	0
D_{11} (N.m^2)	4.6	1.07×10^1	4.6
D_{22} (N.m^2)	5.6×10^1	4.3×10^1	2.0×10^1
D_{33} (N.m^2)	1.0×10^2	7.79×10^1	3.7×10^1

236

237 By evaluating the previous two test cases, it is clear that the developed aeroelastic code is capable of
238 predicting the effect of added mass on the aeroelastic stability of composite hingeless rotor blades in
239 hover. In what follows, the effect of added mass on the twist morphing and the aeroelastic stability of
240 the composite blades is analysed. The blade characteristics are same as the one used in the previous
241 section, except that the layup arrangement here is no longer antisymmetric. This is because here the
242 bend-twist coupling is the main source of the twist morphing, and therefore, a unidirectional laminate
243 consisting of 6 plies with fibre angle ζ in each wall is considered ($[\zeta]_6$). This composite configuration
244 means that the **B** components of the stiffness matrix (Eq. (2)) become zero, while other stiffness
245 values (**A, D**) are non-zero. This is because the lag-torsion coupling is the source of the twist change
246 in this paper. Note that in all cases from here on, the rotor angular velocity is Ω_R=1000 rpm, and it is

assumed that the centroid of the spar box is coincident with centre of mass of the blade at the quarter chord of the NACA 0012 airfoil.

The mass magnitude is considered here as a fraction of the blade mass itself, and denoted as $\mu=m_p/m$. First the effect of added mass on the twist change of the composite blade is examined. In this case, the aerodynamic loading isn't considered. Figure 4 shows the effect of different ply angles on the spanwise twist distribution of the blade for two locations of the mass. The upper domain is for the most aft position of the mass, while the lower domain is for the most forward location of the mass. By introducing the mass, the twist distribution of the blade changes, and the rate of change depends on the ply orientation. By moving the mass from the trailing edge to the leading edge of the cross-section, about $\delta\phi_{tip} = 5.5^o$ tip twist change is induced when the ply angle is ζ=30°.

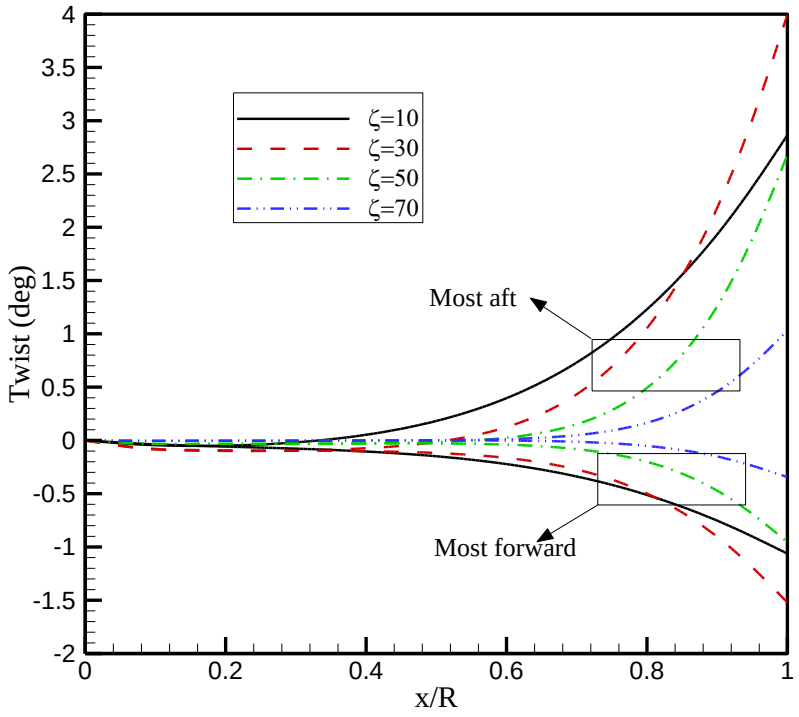

Figure 4: The twist distribution of the blade for different layup angles and two chordwise positions (μ=0.05, x_p/R=1)

The effect of different ply angles on the tip twist value of the blade is determined and shown in Figure 5. Here the spanwise location of the mass is at the tip of the blade. By increasing the ply angle, the tip twist first increases until a ply angle of about ζ=25°, and then decreases. This is true for both

chordwise locations of the mass. This ply angle is representative of the highest bending-twist coupling in the composite blade in this configuration. In should be noted that the ply angle not only changes the lag-torsion coupling but also it influences the rotating frequencies of the blade to some extent.

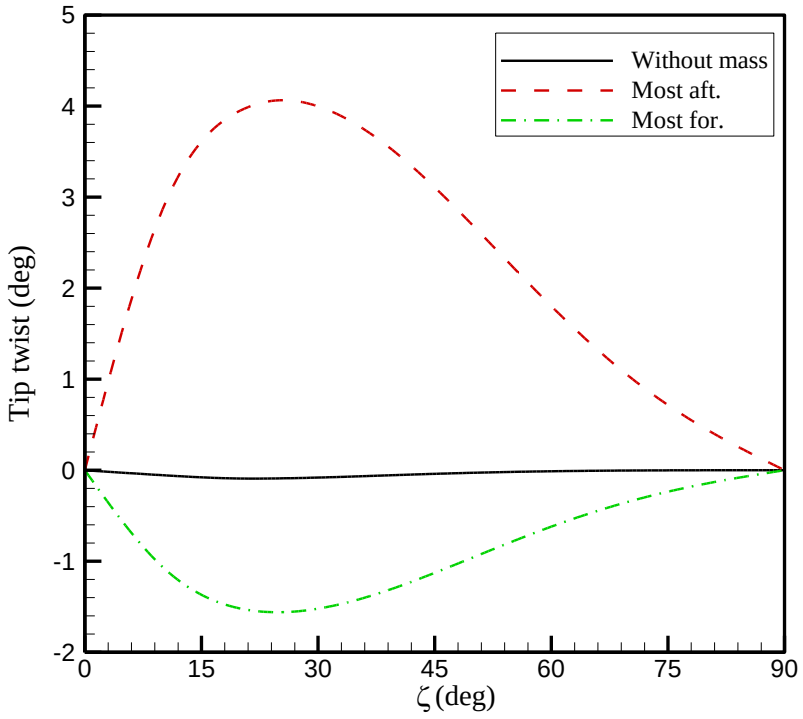

Figure 5: The blade tip twist versus layup angle for (μ=0.05, x_p/R=1)

Figure 6 demonstrates the effect of spanwise location of the point mass on the actuation range of blade tip twist for different layup angles. The actuation range of blade tip twist is the difference of the tip twist between the aft and forward locations of the point mass; and therefore indicates the potential degree to which tip twist may be morphed in flight. The highest tip twist change occurs when the mass is located at the tip of the blade for all ply angles. Moreover, the maximum tip twist change for the spanwsie location of the mass between $0.5<x/R<0.8$ is for $\zeta=10^o$, while from here on to the tip of the blade is for $\zeta=30^o$.

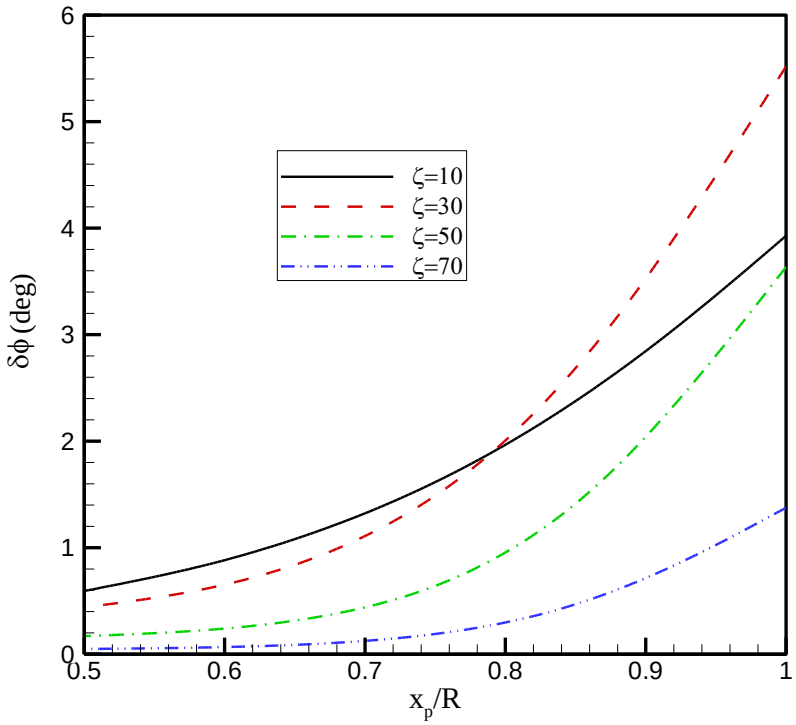

277

278 **Figure 6: The blade tip twist actuation range versus spanwise location for different ply angles (μ=0.05)**

279 Finally, the effect of non-dimensional mass magnitude on the tip twist actuation range of the
280 composite blade is analysed and shown in Figure 7. By increasing the mass magnitude, the amount of
281 twist change increases for all ply angles. By considering all the results presented above, it is
282 highlighted here that the mass magnitude and location affects the twist change of the blade
283 dramatically. Depending on the spar configuration, there is one layup orientation that results in the
284 highest twist change in the blade. Therefore, in terms of the blade twist morphing, moving a mass
285 near the tip of blade has positive effects. Now in the what follows, the effect of the mass on the
286 aeroelastic stability of composite blade is discussed.

287 Figure 8 shows the effect of aerodynamic loads on the tip twist change of the blade when the mass is
288 located at the tip. In this case, the blade pitch angle is zero. It is clear that by adding the aerodynamic
289 loads and moments to the blade, the tip twist decreases. This is because the blade flap angle tends to
290 decrease the lag bending moment applied on the point mass. This highlights the importance of the
291 aerodynamic loads on the effectiveness of this morphing concept.

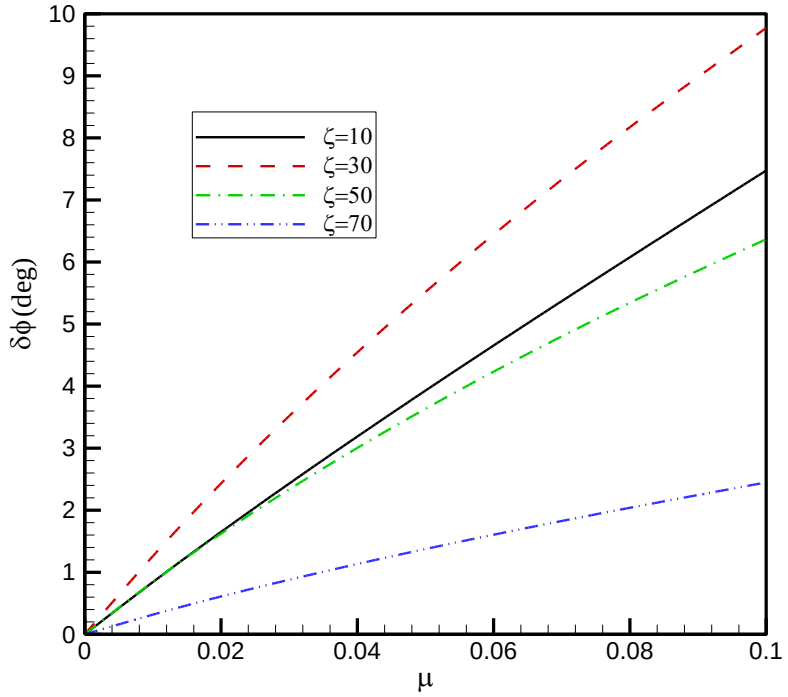

Figure 7: The blade tip twist actuation range versus mass magnitude (x_p/R=1)

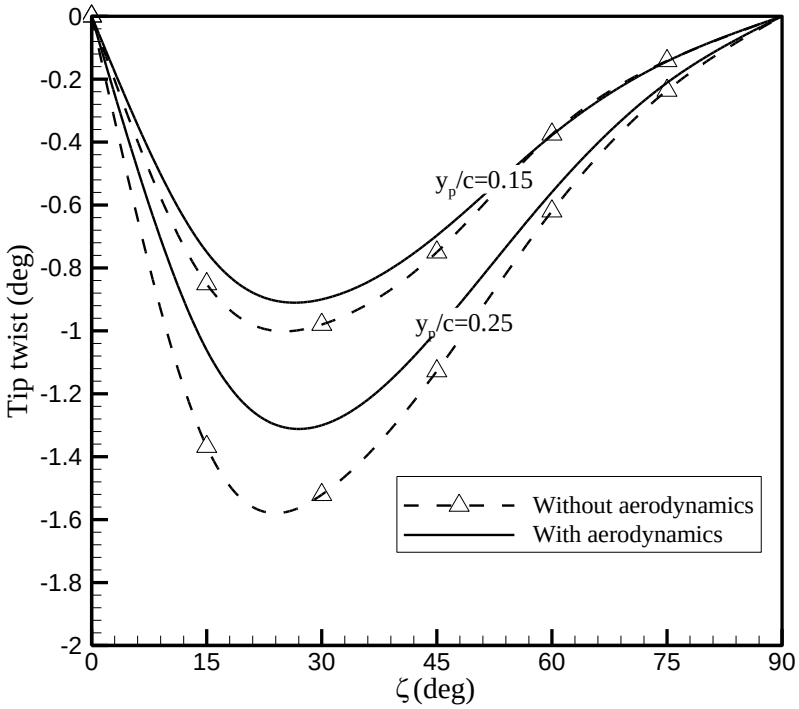

Figure 8: The blade tip twist value with and without aerodynamic loads for different ply angles (μ=0.05, x_p/R=1)

Figure 9 illustrates the aeroelastic stability of the composite blade with respect to different layup angles. In this case the blade does not include any added mass. The blade is stable for ply angles

higher than about $\zeta=65^o$ and smaller than $\zeta=1^o$. The instability domain is almost the same for all layup angles between these two boundaries, but the domain tends to get larger for ply angles between $1^o<\zeta<10^o$. It is noted that as this blade is unstable in the region between $1^o<\zeta<65^o$, and the ply angle that needs to be selected for designing the morphing mechanism must be outside this range. However, it could be possible to design a cross-section to achieve required level of twist change subject to the aeroelastic instability constraints.

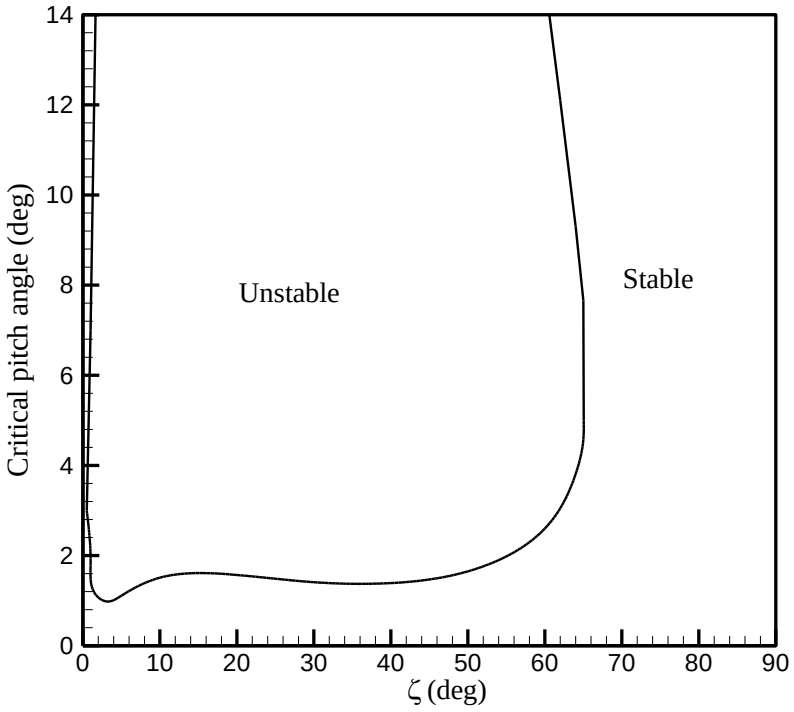

Figure 9: The stability boundary of the composite blade without added mass

The effect of nondimesional mass magnitude on the lead-lag aeroelastic stability boundaries is shown in Figure 10. In this case, the mass is located at the tip of the blade on the shear centre of the section. By increasing the mass magnitude, the unstable region decreases. Therefore, the point mass located at the shear centre of the blade, has a stabilizing effect. The left boundary of the unstable region stays unchanged by the additional mass until $\zeta=40^o$. Moreover, by introducing the mass to the blade, the layup angle that the blade enters into the stable region decreases. Therefore, by adding a mass to the blade and locating it exactly on the elastic axis of the blade, the aeroelastic stability of the blade increases.

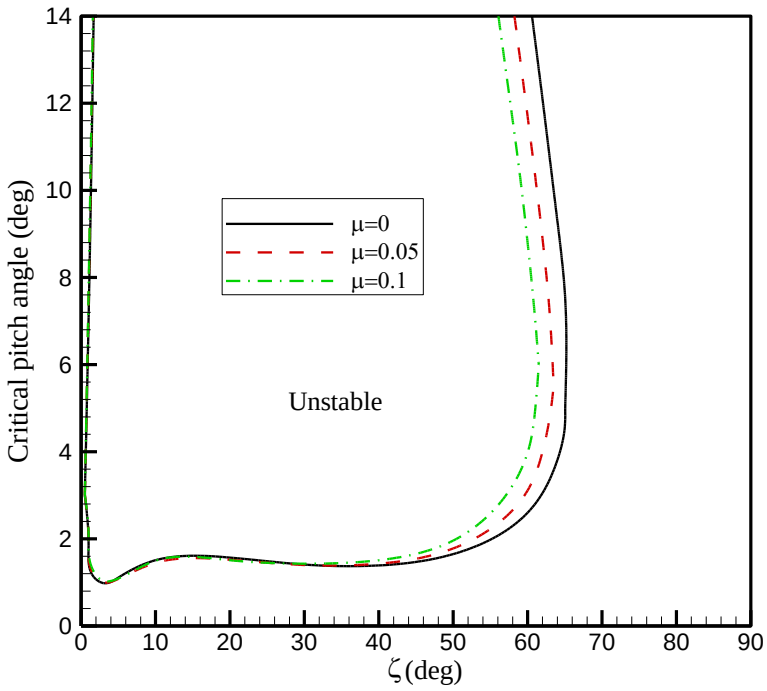

Figure 10: Stability boundaries of the lag mode for different point mass magnitudes (y_p/c=0, x_p/R=1)

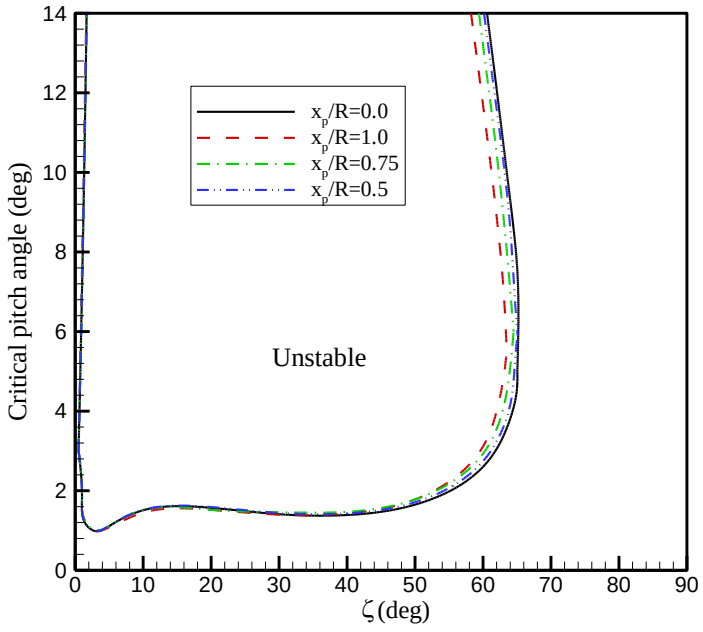

Figure 11: Stability boundaries of the lag mode for different spanwise locations of the point mass (μ=0.05, y_p/c=0)

Figure 11 shows how the spanwise location of the added mass changes the lead-lag aeroelastic stability boundaries. Here, the mass value is 5 percent of the blade weight (μ=0.05) and located at the shear centre of the blade. By moving the mass from the mid-span to the tip of the blade, the unstable region shrinks. It is noted that the point mass spanwise location has a minor effect on the lead-lag aeroelastic instability. This is because the mass doesn't produce any lag moment and therefore, the bend-twist coupling doesn't produce any torsional moment.

The effect of chordwise movement of the point mass on the lead-lag aeroelastic stability of the composite blade is shown in Figure 12. By moving the mass from the leading edge to the trailing edge, the size of the unstable region increases. This indicates that the chordwise location of the mass critically changes the stability characteristics of the blade. Moreover, the ply angle at which the blade enters the stable region increases by moving the mass toward the trailing edge. By moving the mass toward the trailing edge, the lag moment due to the centrifugal force of the added mass, produces a nose up pitching moment which in turn increases the aerodynamic loads. Therefore, moving the mass toward the trailing edge has a destabilizing effect on the blade in this configuration.

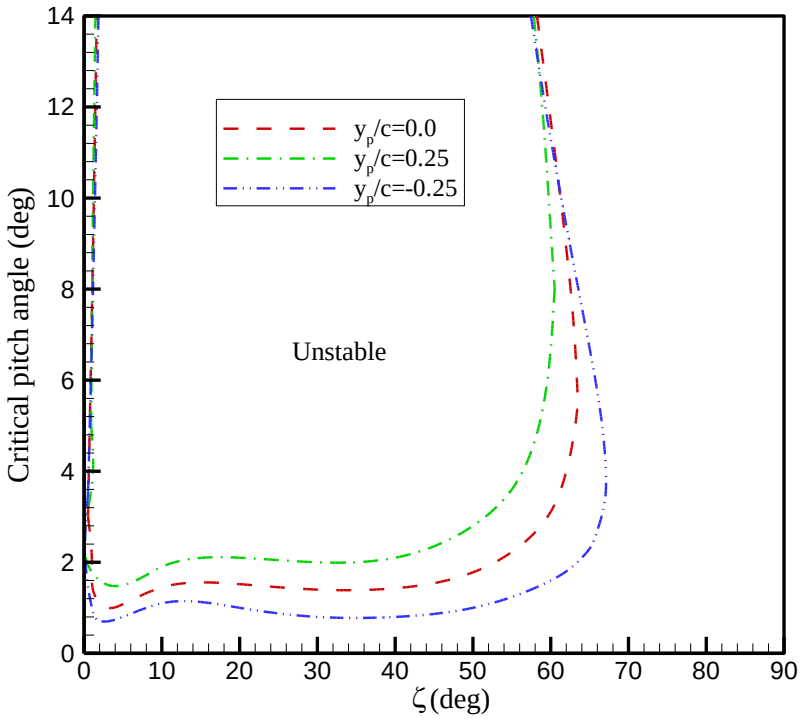

Figure 12: Stability boundaries of the lag mode for different chordwise locations of the point mass (μ=0.05, x_p/R=1)

Finally, the aeroelastic lead-lag damping variation with respect to the blade pitch angle for the above case (y_p/c= -0.25) when the ply angle is ζ=60^o is shown in Figure 13. By increasing the blade pitch, the damping first decreases and then increases. Therefore, the blade pitch angle in this case first has a destabilizing effect and then has a stabilizing effect. This is the reason that in the above cases for a constant ply angle, by increasing the pitch angle, the instability region decreases.

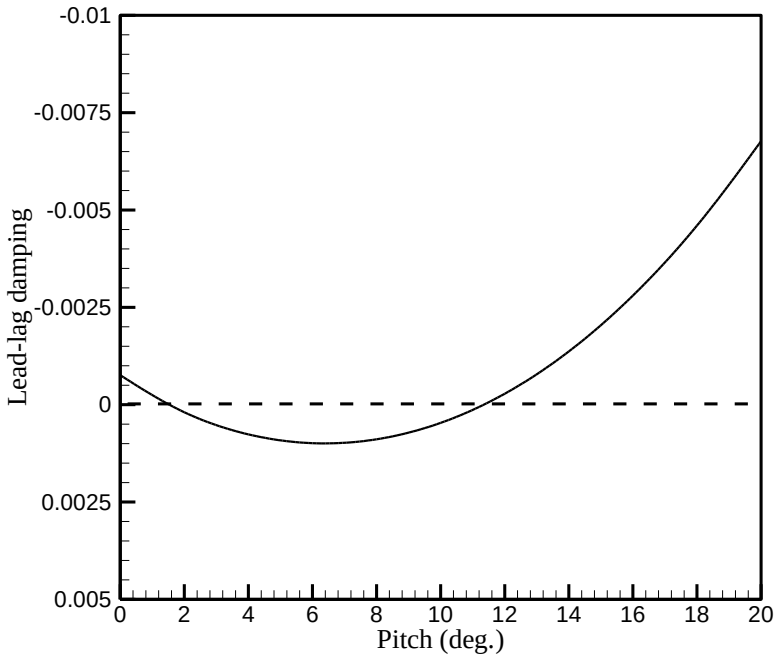

Figure 13: Normalized lead-lag damping for different pitch angles (μ=0.05, x_p/R=1, y_p/c=-0.25, ζ=60^o)

Conclusion

The aeroelastic stability of the a composite hingeless rotor blade with an added mass is studied. The added mass is used as an actuation method to change the twist of the blade. By moving the mass in the chordwise direction, the bending-twist coupling of the composite layup of spar induces a torsional moment on the blade. This torsional moment then changes the twist of the blade. As the added mass may change the aeroelastic stability of the blade, the effect of its spanwise and chordwise location, and also its magnitude, on the blade lead-lag stability boundaries is evaluated. Introducing the mass to the blade, can change the twist distribution of the blade. The amount of twist induced in the blade depends on the layup angle, mass magnitude, mass location, and angular velocity of the rotor. The added mass influences the lead-lag aeroelastic instability of the blade. By moving the mass towards

the tip of the blade, the instability region decreases, while by moving the mass from the leading edge to the trailing edge of the blade, the unstable domain increases. Moreover, the mass magnitude also affects the stability boundaries of the blade. Therefore, this morphing concept may be subjected to aeroelastic instabilities, and in designing or modifying a blade to work with this morphing concept, it is essential to consider the aeroelastic stability as a design constraint.

Acknowledgments

The work presented in this paper was funded by the European Community's Horizon 2020 Program through the project "Shape Adaptive Blades for Rotorcraft Efficiency (SABRE)", Grant Agreement 723491.

References

1. Mistry, M., Gandhi, F., Nagelsmit, M., and Gurdal, Z. "Actuation Requirements of a Warp-Induced Variable Twist Rotor Blade," *Journal of Intelligent Material Systems and Structures* Vol. 22, No. 9, 2011, pp. 919-933.
2. Han, D., Pastrikakis, V., and Barakos, G. N. "Helicopter flight performance improvement by dynamic blade twist," *Aerospace Science and Technology* Vol. 58, 2016, pp. 445-452.
3. Chen, P. C., and Chopra, I. "Induced strain actuation of composite beams and rotor blades with embedded piezoceramic elements," *Smart Materials and Structures* Vol. 5, No. 1, 1996, p. 35.
4. Chen, P. C., and Chopra, I. "Hover Testing of Smart Rotor with Induced-Strain Actuation of Blade Twist," *AIAA Journal* Vol. 35, No. 1, 1997, pp. 6-16.
5. Chattopadhyay, A., Liu, Q., and Gu, H. "Vibration Reduction in Rotor Blades Using Active Composite Box Beam," *AIAA Journal* Vol. 38, No. 7, 2000, pp. 1125-1131.
6. Cesnik, C. E. S., Shin, S., and Wilbur, M. L. "Dynamic response of active twist rotor blades," *Smart Materials and Structures* Vol. 10, No. 1, 2001, p. 62.
7. Shin, S. J., and Cesnik, C. "Forward flight response of the active twist rotor for helicopter vibration reduction," *19th AIAA Applied Aerodynamics Conference*. American Institute of Aeronautics and Astronautics, 2001.
8. Pawar, P. M., and Jung, S. N. "Active twist control methodology for vibration reduction of a helicopter with dissimilar rotor system," *Smart Materials and Structures* Vol. 18, No. 3, 2009, p. 035013.
9. Prahlad, H., and Chopra, I. "Design of a variable twist tilt-rotor blade using shape memory alloy (SMA) actuators," *SPIE's 8th Annual International Symposium on Smart Structures and Materials*, 2001.
10. Amoozgar, M. R., Shaw, A. D., Zhang, J., and Friswell, M. I. "Composite Blade Twist Modification by Using a Moving Mass and Stiffness Tailoring," *AIAA Journal*, Accepted December 2018, DOI: 10.2514/1.J057591.
11. Amoozgar, M. R., Shaw, A. D., Zhang, J., and Friswell, M. I. "Twist morphing of a hingeless rotor blade using a moving mass," *44th European Rotorcraft Forum*. Delft, The Netherlands, 2018.

12. Hodges, D. H., and Ormiston, R. A. "Stability of elastic bending and torsion of uniform cantilever rotor blades in hover with variable structural coupling," *NASA TN D-8192*, 1976.
13. Hodges, D. H. "Review of composite rotor blade modeling," *AIAA Journal* Vol. 28, No. 3, 1990, pp. 561-565.
14. Hong, C., Ho, and Chopra, I. "Aeroelastic Stability Analysis of a Composite Rotor Blade," *Journal of the American Helicopter Society* Vol. 30, No. 2, 1985, pp. 57-67.
15. Panda, B., and chopra, I. "Aeroelastic response, loads, and stability of a composite rotor in forward flight," *Vertica 11 (1/2)*, 1987, pp. 187-209.
16. Smith, E. C., and Chopra, I. "Aeroelastic Response, Loads, and Stability of a Composite Rotor in Forward Flight," *AIAA Journal* Vol. 31, No. 7, 1993, pp. 1265-1273.
17. Kim, T., and Dugundjit, J. "Nonlinear Large Amplitude Aeroelastic Behavior of Composite Rotor Blades," *AIAA Journal* Vol. 31, No. 8, 1993, pp. 1489-1497.
18. Smith, E. C. "Vibration and flutter of stiff-inplane elastically tailored composite rotor blades," *Mathematical and Computer Modelling* Vol. 19, No. 3, 1994, pp. 27-45.
19. Tracy, A. L., and Chopra, I. "Aeroelastic Stability Investigation of a Composite Hingeless Rotor in Hover," *Journal of Aircraft* Vol. 35, No. 5, 1998, pp. 791-797.
20. Jeon, S. M., Cho, M. H., and Lee, I. "Aeroelastic analysis of composite rotor blades in hover," *Computers & Structures* Vol. 66, No. 1, 1998, pp. 59-67.
21. Shang, X., Hodges, D. H., and Peters, D. A. "Aeroelastic Stability of Composite Hingeless Rotors in Hover with Finite-State Unsteady Aerodynamics," *Journal of the American Helicopter Society* Vol. 44, No. 3, 1999, pp. 206-221.
22. Jeon, S. M., and Lee, I. "Aeroelastic response and stability analysis of composite rotor blades in forward flight," *Composites Part B: Engineering* Vol. 32, No. 3, 2001, pp. 249-257.
23. Friedmann, P. P., Yuan, K.-A., and de Terlizzi, M. "An aeroelastic model for composite rotor blades with straight and swept tips. Part I: Aeroelastic stability in hover," *International Journal of Non-Linear Mechanics* Vol. 37, No. 4, 2002, pp. 967-986.
24. Bao, J., Nagaraj, V. T., Chopra, I., and Bernhard, A. "Design and Hover Test of Low Vibration Mach Scale Rotor with Twisted Composite Tailored Blade," *44th AIAA/ASME/ASCE/AHS/ASC Structures, Structural Dynamics, and Materials Conference*. American Institute of Aeronautics and Astronautics, 2003.
25. Friedmann, P. P., Glaz, B., and Palacios, R. "A moderate deflection composite helicopter rotor blade model with an improved cross-sectional analysis," *International Journal of Solids and Structures* Vol. 46, No. 10, 2009, pp. 2186-2200.
26. Fulton, M. V., and Hodges, D. H. "Aeroelastic stability of composite hingeless rotor blades in hover—Part II: Results," *Mathematical and Computer Modelling* Vol. 18, No. 3, 1993, pp. 19-35.
27. Lim, I.-G., and Lee, I. "Aeroelastic analysis of bearingless rotors with a composite flexbeam," *Composite Structures* Vol. 88, No. 4, 2009, pp. 570-578.
28. Xiao, Y., Xu, G. H., and Zhao, Q. J. "Aeroelastic stability analysis of composite hingeless rotor based on free-wake model," *Hangkong Dongli Xuebao/Journal of Aerospace Power* Vol. 28, No. 5, 2013, pp. 1086-1094.
29. Byers, L., and Gandhi, F. "Embedded absorbers for helicopter rotor lag damping," *Journal of Sound and Vibration* Vol. 325, No. 4, 2009, pp. 705-721.
30. Byers, L., and Gandhi, F. "Rotor blade with radial absorber (Coriolis damper)- Loads evaluation," *Presented at the American Helicopter Society 62nd Annual Forum, Phoenix, AZ*, 2006.
31. Byers, L., and Gandhi, F. "Helicopter rotor lag damping augmentation based on a radial absorber and coriolis coupling," *Presented at the American Helicopter Society 61st Annual Forum, Grapevine, TX*, 2005.

32. Kang, H., Smith, E. C., and Lesieutre, G. A. "Experimental and Analytical Study of Blade Lag Damping Augmentation using Chordwise Absorbers," *Journal of Aircraft* Vol. 43, No. 1, 2006, pp. 194-200.
33. Hodges, D. H. "Geometrically Exact, Intrinsic Theory for Dynamics of Curved and Twisted Anisotropic Beams," *AIAA Journal* Vol. 41, No. 6, 2003, pp. 1131-1137.
34. Amoozgar, M. R., Shahverdi, H., and Nobari, A. S. "Aeroelastic Stability of Hingeless Rotor Blades in Hover Using Fully Intrinsic Equations," *AIAA Journal* Vol. 55, No. 7, 2017, pp. 2450-2460.
35. Yu, W., Hodges, D. H., Volovoi, V., and Cesnik, C. E. S. "On Timoshenko-like modeling of initially curved and twisted composite beams," *International Journal of Solids and Structures* Vol. 39, No. 19, 2002, pp. 5101-5121.
36. Amoozgar, M. R., and Shahverdi, H. "Analysis of nonlinear fully intrinsic equations of geometrically exact beams using generalized differential quadrature method," *Acta Mechanica* Vol. 227, No. 5, 2016, pp. 1265-1277.
37. Sotoudeh, Z., and Hodges, D. H. "Structural Dynamics Analysis of Rotating Blades Using Fully Intrinsic Equations, Part I: Formulation and Verification of Single-Load-Path Configurations," *Journal of the American Helicopter Society* Vol. 58, No. 3, 2013, pp. 1-9.
38. Sachdeva, C., Gupta, M., and Hodges, D. H. "Modeling of initially curved and twisted smart beams using intrinsic equations," *International Journal of Solids and Structures* Vol. 148-149, 2017, pp. 3-13.
39. Gessow, A., and Mayers, G. C., Jr. *Aerodynamics of the Helicopter*. Fredrick Ungar Publishing Company, New York, New York, 1967
40. Wright, A. D., Smith, C. E., Thresher, R. W., and Wang, J. L. C. "Vibration Modes of Centrifugally Stiffened Beams," *Journal of Applied Mechanics* Vol. 49, No. 1, 1982, pp. 197-202.